Enhanced high-altitude polar cap plasma and magnetic field values in response to the interplanetary magnetic cloud that caused the great storm of 31 March 2001: A case study for a new magnetospheric index

Vladimir A. Osherovich,[1,2] Robert F. Benson,[2] Joseph Fainberg,[2] James L. Green,[3] Leonard Garcia,[2,4] Scott Boardsen,[2,5] Nikolai Tsyganenko,[2,6] and Bodo W. Reinisch[7]

Received 5 October 2006; revised 19 March 2007; accepted 30 March 2007; published 29 June 2007.

[1] The magnetospheric electron number density and the magnetic field strength near 8 R_E over the polar cap increased dramatically after the arrival of an interplanetary magnetic cloud on 31 March 2001. These parameters were determined with high accuracy from the plasma resonances stimulated by the Radio Plasma Imager (RPI) on Imager for Magnetopause-to-Aurora Global Exploration (IMAGE) near apogee during both quiet (30 March 2001) and disturbed (31 March 2001) days. The quiet day and disturbed day values were each compared with magnetospheric magnetic field and electron density models; good agreement was found with the former but not the latter. The magnetospheric response was also expressed in terms of the ratio of the electron plasma frequency f_{pe} to the electron cyclotron frequency f_{ce}, which is proportional to the ratio of the electron gyroradius to the Debye radius. Simultaneous Wind measurements of the solar wind magnetic field strength, speed, and plasma density were used to calculate the solar wind quasi-invariant QI. This index is equivalent to the ratio of the solar wind magnetic pressure to the solar wind ram pressure or to the inverse of the magnetic Mach number squared. These nondimensional quantities, QI and f_{pe}/f_{ce}, have fundamental meanings in the solar wind MHD regime and in the relation between electric and magnetic forces on electrons in the magnetosphere, respectively. During the large 31 March 2001 storm, IMAGE was at the right place at the right time so as to enable comparisons between RPI f_{pe}/f_{ce} and Wind QI determinations. Both QI and f_{pe}/f_{ce} formed maxima during 6-hour observing intervals during this storm that were found to be highly correlated (87%) with a magnetospheric time lag of about 3 hours for f_{pe}/f_{ce}. These results, based on a detailed case study of this important event, suggest that the plasma parameter f_{pe}/f_{ce} may serve as a useful magnetospheric index.

Citation: Osherovich, V. A., R. F. Benson, J. Fainberg, J. L. Green, L. Garcia, S. Boardsen, N. Tsyganenko, and B. W. Reinisch (2007), Enhanced high-altitude polar cap plasma and magnetic field values in response to the interplanetary magnetic cloud that caused the great storm of 31 March 2001: A case study for a new magnetospheric index, *J. Geophys. Res.*, *112*, A06247, doi:10.1029/2006JA012105.

1. Introduction

1.1. Motivation

[2] While magnetospheric spacecraft routinely make accurate measurements of the terrestrial magnetic field **B**, the same cannot be said for the electron number density N_e. Yet an accurate knowledge of the magnetospheric N_e is important because (1) it is necessary for a proper understanding of the dynamics of large-scale magnetospheric phenomena [e.g., see *Seki et al.*, 2003], (2) it is fundamental to instability growth rate calculations of electron cyclotron harmonic waves that are considered to be a scattering source of diffuse auroral electrons into the loss cone [e.g., see *Horne et al.*, 2003], and (3) N_e may have a significantly greater response than $|\mathbf{B}|$ to interplanetary disturbances as indicated by the case study corresponding to the great storm of 31 March 2001 presented in this paper.

[3] The difficulty in making reliable magnetospheric N_e measurements is well known, particularly under low-density conditions, e.g., $N_e < 1$ cm^{-3}, as has been summarized in section 5 of *Benson et al.* [2001]. Here we determine N_e from accurate measurements of the electron plasma fre-

[1]Catholic University of America, Washington, D.C., USA.
[2]NASA Goddard Space Flight Center, Greenbelt, Maryland, USA.
[3]NASA Headquarters, Washington, D.C., USA.
[4]Perot Systems, Plano, Texas, USA.
[5]University of Maryland Baltimore County, Baltimore, Maryland, USA.
[6]Universities Space Research Association, Columbia, Maryland, USA.
[7]University of Massachusetts Lowell, Lowell, Massachusetts, USA.

0148-0227/07/2006JA012105

quency f_{pe}, i.e., within a few percent, during active Radio Plasma Imager (RPI) resonance soundings from the Imager for Magnetopause-to-Aurora Global Exploration (IMAGE) satellite [*Burch*, 2000] as described by [*Benson et al.*, 2003]

$$f_{pe}(\mathrm{kHz}) \approx \left\{80.6\, N_e\left(\mathrm{cm}^{-3}\right)\right\}^{1/2}. \quad (1)$$

[4] Since IMAGE did not carry a scientific magnetometer, accurate determinations of $|\mathbf{B}|$ (within a few tenths of a percent) were made from the stimulated plasma resonances at the harmonics of the electron cyclotron frequency f_{ce} *Benson et al.* [2003] where f_{ce} is given by

$$f_{ce}(\mathrm{kHz}) \approx 0.028|\mathbf{B}(\mathrm{nT})|. \quad (2)$$

These equations indicate that values of N_e = 1, 10, and 30 cm^{-3} correspond to f_{pe} = 9, 28, and 50 kHz, respectively, and a value of $|\mathbf{B}|$ = 100 nT corresponds to f_{ce} = 2.8 kHz.

[5] In this paper the great magnetic storm of 31 March 2001 was used as a case study to relate a disturbance in the interplanetary medium, namely a magnetic cloud, as measured by the Wind satellite to changes in physical parameters in the polar cap as measured by RPI on the IMAGE satellite. These physical parameters are N_e and $|\mathbf{B}|$ as reflected in the measured f_{pe} and f_{ce} of equations (1) and (2). They were determined simultaneously both on the disturbed day of 31 March and, as a point of comparison, on the quiet day of 30 March. As in the work of *Benson et al.* [2001], we stress the importance of the nondimensional magnetospheric parameter f_{pe}/f_{ce}. Our goal is to relate this parameter to a new nondimensional heliospheric index, i.e., the solar wind QI [*Osherovich et al.*, 1999b], in order to characterize the impact of a magnetic cloud on the magnetosphere.

1.2. Solar Wind Quasi-Invariant (QI)

[6] Since solar activity involves changes on the Sun and the solar wind with consequences in the Earth's magnetosphere, an understanding of magnetic storms requires us to monitor, and relate the changes between, three magnetized plasmas. Any predictive technique relies on the ability to describe the entire process. The forecasting of solar activity is possible only because of existing indices. Three solar indices are shown in Figures 1a and 1b corresponding to a 2000-day time interval (approximately from solar maximum to solar minimum) [*Pap et al.*, 1997]. Traditionally, solar cycles are depicted by the variation in the sunspot number (SSN). Both the SSN and the closely correlated 10.7-cm radio flux (shown in Figure 1b) are global indices; the correlation coefficient (cc) between them is 0.99. They are obtained by integration over the entire solar disc. The other two solar indices, shown in Figures 1a, are also global indices. They are the Solar Ultraviolet Spectral Irradiance Monitor (SUSIM) Mg c/w index and the Active Cavity Radiometer Irradiance Monitor (ACRIM) II total irradiance corrected for sunspot darkening (Figure 1a). Like many other solar indices, they are related to different aspects of activity observed on the Sun (see review by *Hathaway* [1998]).

[7] Geomagnetic indices are a second class of indices. They reflect the reaction of the Earth's magnetosphere and ionosphere to interplanetary disturbances and are known to be dependent on the solar cycle [*Cliver et al.*, 1999, and references therein]. Traditionally, the magnetosphere/ionosphere response to changing solar wind conditions is described in terms of coupling functions between solar wind parameters and geomagnetic indices such as *Kp*, *Dst*, *aa*, etc.; see, e.g., the list of proposed coupling functions given in Table 1 of *Stamper et al.* [1999] and the reviews by *Feynman* [1983] and *Baker* [1986]. The relationship of the geomagnetic indices to fundamental magnetospheric parameters is a difficult problem in itself.

[8] Physical parameters measured by spacecraft in the solar wind can be used to construct a third class of indices, namely solar wind indices. Gauging the solar cycle by solar wind parameters such as the interplanetary magnetic field strength B [*King*, 1979; *Slavin et al.*, 1986], plasma density ρ, and bulk speed v has certain advantages since the theory of the solar wind is formulated in terms of these physical parameters. The main disadvantage is the low correlation obtained between them taken individually (especially for ρ and v) and the SSN. We define a quasi-invariant (QI) as a combination of physical parameters that has a significantly higher correlation with some index than the correlations obtained by considering each component taken separately with the same index. Such a solar wind QI, based on a combination of B, ρ, and v, has been shown to have a high correlation coefficient with SSN (cc = 0.98) for yearly median values over an interval of nearly 3 solar cycles [*Osherovich et al.*, 1999b]. It is given by

$$\mathrm{QI} = \left(B^2/8\pi\right)/\left(\rho v^2/2\right) = \left(1/M_A\right)^2 \quad (3)$$

where M_A is the solar wind magnetic Mach number. Other combinations of solar wind parameters were found to have significantly lower correlations with SSN. In this regard, QI is the best indicator to date of solar activity based solely on spacecraft measurements. Figure 1c presents running 55- and 27-day averages of QI for the same time interval as used by *Pap et al.* [1997] in Figures 1a and 1b. A comparison between Figures 1b and 1c shows that even for these intermediate timescales, QI is still a good representation of the solar activity. For the time interval in Figure 1 the running averages of QI correlate with the 10.7-cm radio flux with cc = 0.85 and 0.79 for 55- and 27-day averages, respectively.

[9] The helium abundance, defined as the helium-to-proton number-density ratio He/N_p, was assumed to be the standard 0.05 in the determination of the ρ value used in (3) to calculate the QI displayed in the intermediate timescales of Figure 1c. A quantitative analysis relating variations in the solar wind QI and magnetospheric parameters, however, requires the use of a ρ value based on the observed variations in the helium abundance rather than one based only on the variations in N_p and a fixed He/N_p ratio, particularly when magnetic clouds, known to be anomalously rich in He (see Figure 2c), are involved. (The abundance of additional elements other than He in the solar atmosphere is below one percent and has little impact on the calculation of ρ [*Allen*, 1973].) This procedure was used in the calculation of QI presented in Figure 2b for a 30-day time interval that includes the 30–31 March 2001 period of interest in the present work. This period is identified with the onset of a huge drop in *Dst* to values lower than −300, beginning on

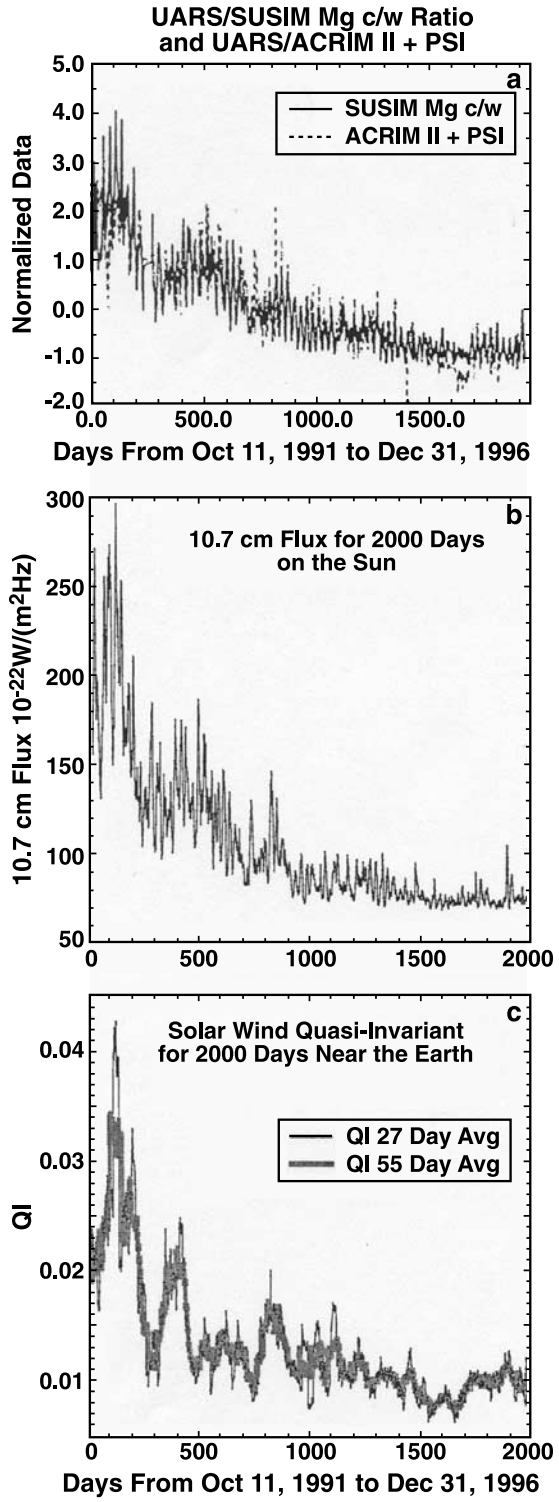

Figure 1. (a) Solar Ultraviolet Spectral Irradiance Monitor (SUSIM) Mg c/w and Active Cavity Radiometer Irradiance Monitor (ACRIM) II total irradiance values corrected for sunspot darkening (after *Pap et al.* [1997]), (b) 10.7 cm flux (after *Pap et al.* [1997]), (c) quasi-invariant (QI) for the same time interval correlates with the 10.7 cm flux with cc = 0.85 and 0.79 for the 55-day and 27-day running averages, respectively.

Day 90 as shown in Figure 2a. This large decrease is attributed to the impact of a magnetic cloud on the magnetosphere. Two other significant decreases in *Dst* identified in this figure are similarly attributed to magnetic cloud impacts. Among the characteristics of magnetic clouds are enhanced $|\mathbf{B}|$ and often decreased ρ due to expansion (see, e.g., the review by *Osherovich and Burlaga* [1997] and references therein). It has recently been shown that due to these two factors in equation (3), all magnetic clouds have enhancements of QI by a factor of 10 to 100 relative to normal solar wind values, i.e., magnetic clouds represent a gross violation of the regular quasi-invariant [*Osherovich et al.*, 1999a, 1997]. Other geoeffective structures, e.g., noncloud ejecta and corotating streamers, may also have high QI. A sheath surrounds a typical cloud, with enhanced ρ, due to the shocks preceding and following it. These characteristics are most clearly seen in the signature of the magnetic cloud centered on day 79 in Figure 2. Here, coinciding with the decrease in *Dst*, is an increase in QI (Figure 2b) and B (Figure 2d), a decrease in *Bz* (Figure 2e), a decrease in N_p (Figure 2f) preceded and followed by shock-driven enhancements, and the typical signature of expansion relative to the center of the cloud, i.e., a decreasing slope in the measured v as the cloud moves past the spacecraft (Figure 2g).

[10] Figure 2 illustrates that QI is an essential player in identifying disturbances in the solar wind that lead to large magnetic storms. The three outstanding peaks in QI correspond to three magnetic clouds. In contrast, B, N_p, and v taken separately have 6 to 7 outstanding peaks. The same is true for *Bz*. The approximate timing and relative amplitude of these three peaks in QI illustrate the value of QI as an indicator of large decreases in *Dst* associated with magnetic storms (compare Figures 2a and 2b). The shorter duration of QI relative to *Dst* suggests that QI can be considered a trigger of the magnetic storm which persists for a longer time as expressed by the tail in the *Dst* recovery. It is important to note that the same solar wind parameter QI, which closely follows the solar cycle, also provides a quantitative measure of short-term solar wind disturbances, causing large magnetic storms. While all of the solar wind parameters shown in Figure 2 are solar cycle-dependent to some degree, we are not aware of any combination of these parameters that can closely accommodate both a long-term association with solar indices (such as the SSN or the 10.7 cm flux) and a short-term association with magnetic clouds (that lead to large magnetic storms) as well as the nondimensional QI. Thus QI can be considered as a solar wind benchmark that carries all the information about the solar cycle in its yearly average and also serves as a sensitive indicator (anomalous increases by a factor of 10 to 100) of geomagnetically effective disturbances such as interplanetary magnetic clouds.

[11] Our goal is to identify an equally useful nondimensional parameter in Earth's magnetosphere that reflects the magnetic and plasma response to a QI anomaly in the solar wind. In the next two sections we will present evidence that accurate magnetospheric N_e and $|\mathbf{B}|$ measurements, via f_{pe} and f_{ce} in equations (1) and (2), are sufficient for this goal.

2. IMAGE/RPI Magnetospheric Parameters

[12] Our emphasis is in the outer magnetosphere because RPI typically operates in a high-frequency-resolution mode,

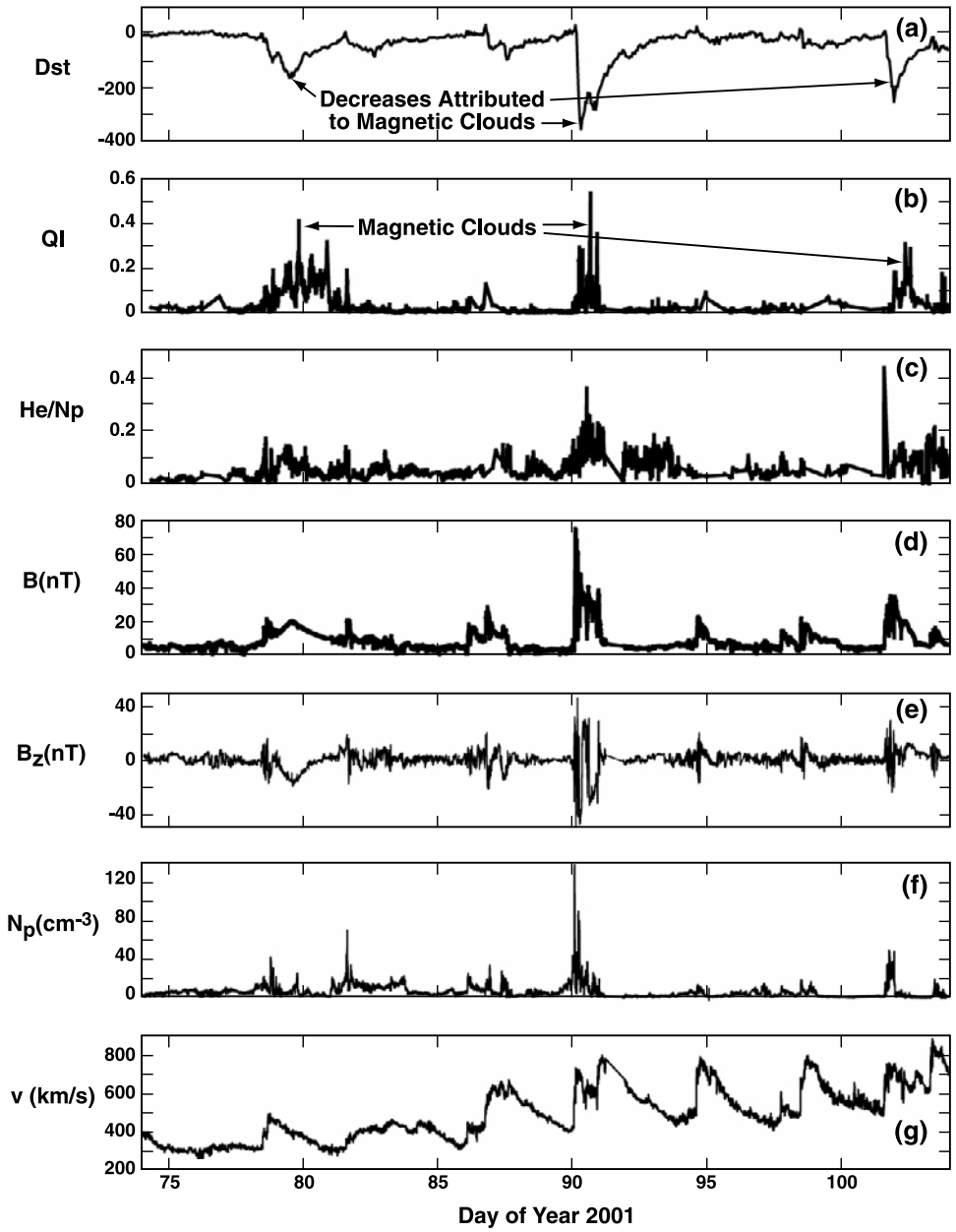

Figure 2. (a) The 30-day interval of *Dst* including the great magnetic storm of 31 March 2001 (day 90). (b–g) QI and solar-wind physical parameters as determined from Wind data available from the Wind project page.

which enables accurate N_e and $|\mathbf{B}|$ determinations to be made, for many hours near apogee ($\approx$8 R_E radial distance) on each IMAGE orbit. In addition, comparisons of these parameters near apogee on successive orbits allow variations due to changing magnetic conditions to be investigated while minimizing the effect of the large variations in these parameters along the orbit from apogee to perigee. This comparison is illustrated in Figure 3 with active and passive observations before and during the large magnetic storm of 31 March 2001. Figure 3a and 3c display 14 1/2 hours of passive data to cover a full orbit of IMAGE while Figures 3b and 3d display enlarged portions of the passive data with superimposed f_{pe} and f_{ce} values determined from plasma-resonance scaling during active operations. The red traces represent f_{ce} based on the T96 model [*Tsyganenko*, 1995, 1996; *Tsyganenko and Stern*, 1996] and the white traces represent f_{pe} based on a composite of various magnetospheric models which reduces to the *Persoon et al.* [1983] model in the polar cap. The sharp enhancement of the white trace (f_{pe}) just prior to 1830 and the longer-duration enhancement near 2030 in Figure 3d result from a modeled magnetosheath location (based on *Roelof and Sibeck* [1993]) inside the position of the IMAGE satellite, i.e., these large f_{pe} values correspond to magnetosheath estimates rather than to the magnetospheric f_{pe} model. Neither the dynamic spectrum nor the plasma resonance-determined f_{pe} values in Figure 3, however, indicate that IMAGE entered the magnetosheath at these times. The above models

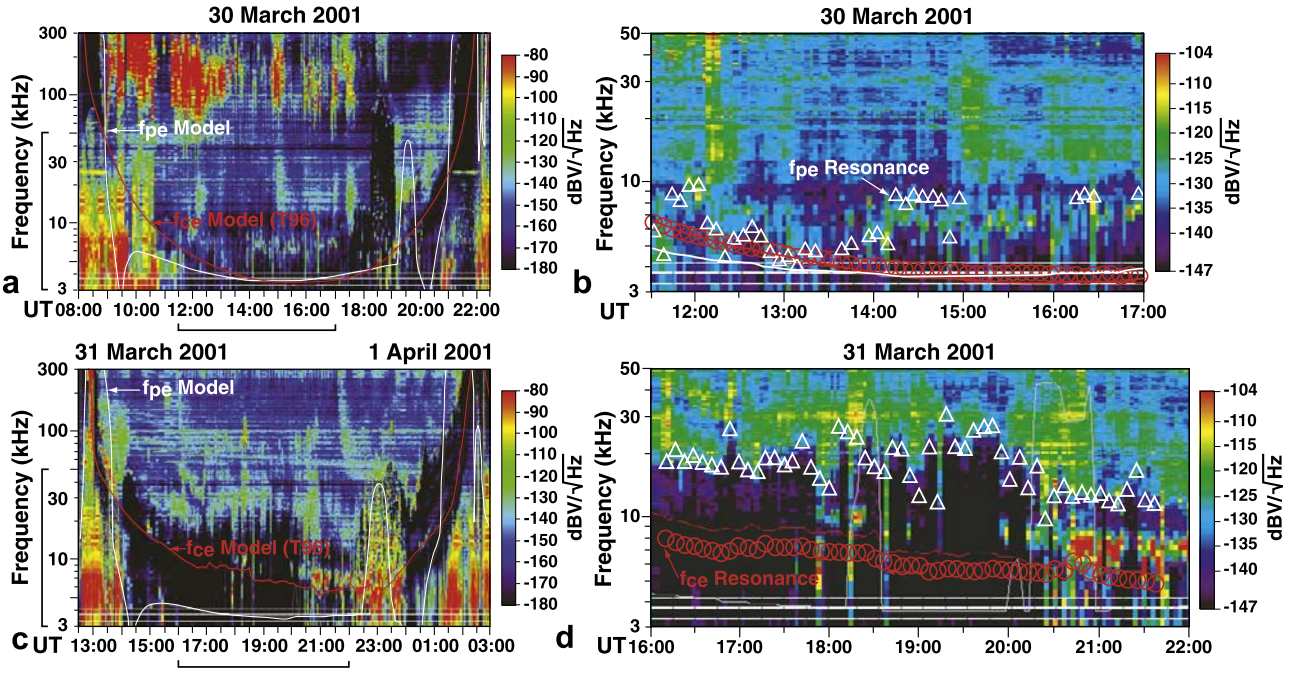

Figure 3. Radio Plasma Imager (RPI) Imager for Magnetopause-to-Aurora Global Exploration (IMAGE) dynamic spectra for (a, c) quiet and (b, d) disturbed days. The vertical and horizontal brackets along the scales on Figures 3a and 3c indicate enlarged portions displayed to the right where f_{pe} and f_{ce} values determined from plasma resonances stimulated during active operations have been superimposed. There are four larger inverted white triangles between 1300 and 1400 UT in Figure 3b that correspond to upper limits for f_{pe} (see Figure 6 caption).

are routinely used to calculate the position of IMAGE relative to the magnetopause and to display f_{ce} and f_{pe} on RPI data records in the analysis program BinBrowser [*Galkin et al.*, 2001].

[13] Major differences are seen in the dynamic spectra between the quiet and disturbed conditions reflecting important physical changes in the state of the magnetosphere. There is a blanking out of continuum radiation up to about 20 kHz (or higher) from approximately 1400 to 2100 UT on the disturbed day (Figure 3c) indicating a large increase in N_e relative to conditions on the quiet day (Figure 3a). This increase in N_e is also clearly evident in the increase in f_{pe}, determined from active resonance soundings, which closely tracks the lower-frequency continuum cutoff (Figure 3d). There is also an intense natural emission in the frequency range between f_{ce} and f_{pe} after about 2040 in Figure 3d. The physical nature of this emission will be discussed in a separate paper.

[14] The f_{pe} and f_{ce} resonance sounding values in Figures 3b and 3d were determined from active sounding records, called plasmagrams, which display the color-coded amplitude and the virtual range of the received echo as a function of sounder frequency. (The virtual range scale corresponds to propagation at the free space speed of light; see *Reinisch et al.* [2000] for a description of the RPI and its data formats.) Examples of these plasmagrams and the plasma resonances stimulated by RPI near apogee are presented in Figure 4. The quiet day plasmagram (Figure 4a) reveals a spectral pattern dominated by nf_{ce} resonances. The disturbed-day plasmagram (Figure 4b) reveals a spectral pattern of RPI-stimulated plasma resonances that is quite different. In either case, f_{pe} is often primarily determined by the identification of the sounder-stimulated resonance at the upper-hybrid frequency f_{uh} where

$$f_{uh}^2 = f_{pe}^2 + f_{ce}^2. \tag{4}$$

The f_{uh} determination was, in turn, aided by the identification of sequences of sounder-stimulated resonances observed between the nf_{ce} plasma resonances above and below f_{uh} known as the *Qn* and *Dn* resonances, respectively [*Benson et al.*, 2003].

[15] A series of RPI plasmagrams, corresponding to a subset of the data used to obtain the f_{pe} and f_{ce} resonance-sounding values superimposed on the RPI passive dynamic spectra in Figure 3d, are presented in Figure 5. The frequencies in each plasmagram have been normalized by f_{ce} as determined from the sequence of sounder-stimulated nf_{ce} plasma resonances. These normalized plasmagrams have been ordered (from top to bottom) by increasing f_{pe}/f_{ce} values where the required f_{pe} value was also determined from sounder-stimulated plasma resonances [*Benson et al.*, 2003]. While the spectral pattern is mainly dictated by the f_{pe}/f_{ce} value [*Benson et al.*, 2003] the intensity and time durations of the resonances, as in the ionosphere [*Benson*, 1972, 1982], is also dependent on other factors.

[16] The labels for the features on the normalized plasmagrams in Figure 5 correspond to a mixture of scaled and calculated values. The first step was to determine the best value for f_{ce} from the observed nf_{ce} resonances (only the resonances up to $n = 6$ appear in Figure 5). Second, the resonances that best matched f_{pe} and f_{uh}, using (4) with

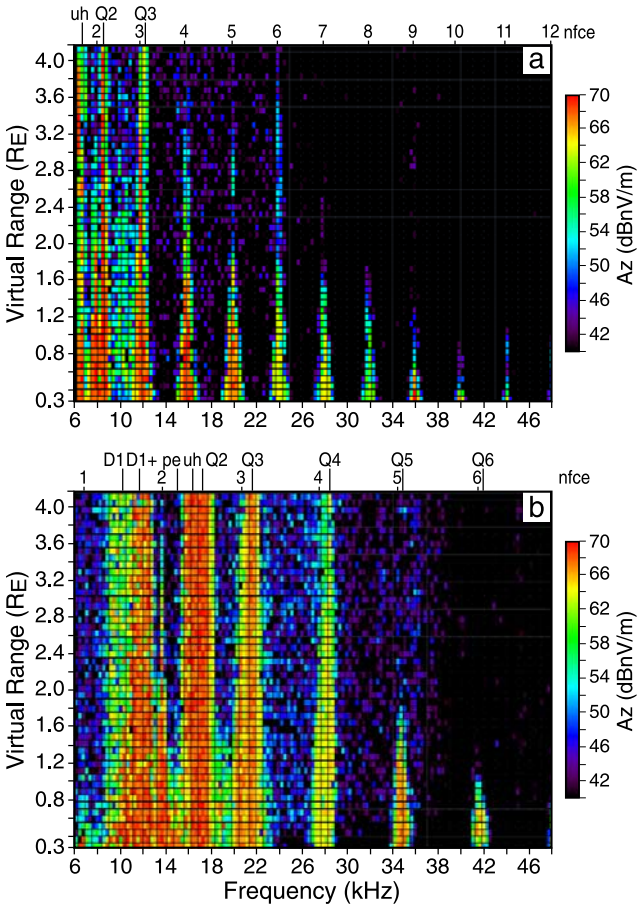

Figure 4. RPI/IMAGE plasmagrams for (a) quiet (30 March 2001 1355 UT) and (b) disturbed (31 March 1753 UT) days as recorded on the *Z* antenna. The subscripts for the frequency designations of the plasma resonances are identified at the top of each figure except for the nf_{ce} resonances which are identified by the appropriate *n* value.

the f_{ce} determined from the first step, were identified. As seen in Figure 5, a resonance was not always observed corresponding to f_{pe} (see, e.g., Figures 5b and 5f). The data in Figure 5 correspond to signals received on the *Z* antenna. The resonance identifications were based on inspecting data from all three of the mutually orthogonal dipole antennas because sometimes a feature would be observed on one but not on the others. In addition, as stated above, the *Qn* and *Dn* sequences aided in this identification of the f_{pe} and f_{uh}, resonances. The third step was to use these scaled f_{pe} and f_{ce} values to calculate the expected locations of the *Dn* and *Qn* resonances as described by *Benson et al.* [2003]. The calculated *Qn* frequencies, based on a Maxwellian electron-velocity distribution, are often higher than the observed resonance frequencies, e.g., compare the calculated positions for *Q*3 and *Q*4 with the observed resonances in Figure 5b. Such frequency discrepancies can be significantly reduced when the *Qn* calculations are based on a Kappa electron-velocity distribution [*Viñas et al.*, 2005].

[17] The main point from the above discussion is that it is the presence of multiple resonance features in Figure 5 that provides confidence in the correct identification of the nf_{ce} resonances and the f_{uh} resonance. Following these identifications, f_{pe} is calculated using (4). Additional confidence is obtained when the calculated f_{pe} is identified with a prominent observed resonance feature as in Figures 5c and 5e. It is the combination of this spectral redundancy and the high-frequency resolution mode of operation (0.3 kHz frequency steps) that enabled accurate determinations of f_{ce} and f_{pe}. Since these resonant phenomena pertain to a large volume (hundreds of meters to kilometers) around the sounder antenna, they are not seriously affected by spacecraft/plasma interactions [*Benson*, 1977] and are considered to be the standard to which direct particle measurement techniques in the ionosphere are compared [*Donley et al.*, 1969] and to provide the starting point for magnetospheric measurements of remote N_e profiles [*Reinisch et al.*, 2001].

[18] These resonance-determined f_{pe} and f_{ce} values over the polar cap on the above quiet and disturbed days presented in Figures 3b and 3d are compared with model values in Figure 6. In Figures 6a and 6c the model for f_{ce} is based on the TS04 model [*Tsyganenko and Sitnov*, 2005], which is suitable for magnetic storms as well as quiet conditions; the f_{ce} comparisons are presented as a percent difference. The model values are within 15% of the observations (which are accurate to much better than 1%) on both days. (Note that the differences can reach 30% if the T96 model, appropriate for quiet conditions, is used for the disturbed day.) The resonance-determined f_{pe} values are compared with the same f_{pe} model values used in Figure 3 as a ratio in Figure 6b. The differences can exceed a factor of 2 on the quiet day and a factor of 8 (or more than a factor of 60 in the ratio of N_e) on the disturbed day, clearly demonstrating the need for accurate f_{pe} values in the distant magnetosphere, particularly on highly disturbed days. The observed and model f_{pe}/f_{ce} values are compared in Figure 6c. The anomalous disturbed-day values involving f_{pe} (model) in Figures 6b and 6c, near 1830 and 2030 are due to the modeled magnetopause position as described in the first paragraph of this section.

[19] Such comparisons between the measured values on the quiet and disturbed days have meaning because the data during the time intervals represented on each of the days in Figure 6 were collected over similar orbital sections as illustrated in Figure 7. The plasmagrams illustrated in Figures 4a and 4b were recorded at similar orbital locations on the 2 days, namely, near 1400 and 1800 UT in Figures 7a and 7b, respectively. Thus it is clear that both the f_{pe} and f_{ce} values increased significantly near the 8 R_E apogee over the polar cap as a result of the magnetic storm. The increase in f_{ce} was significant but typically less than a factor of 2 (compare the red circles in Figures 3b and 3d), while the increase in f_{pe} was often more than a factor of 2 and sometimes a factor of 3 (compare the white triangles in Figures 3a and 3c). Thus there were dramatic differences in the outer magnetospheric polar cap plasma conditions on these 2 days and they were much more pronounced in f_{pe} than in f_{ce}. In this regard it is important to recall that $N_e \propto f_{pe}^2$, indicating that N_e increased by about an order of magnitude in this region as a result of the great magnetic storm on 31 March 2001. The work of *Tu et al.* [2007], using field-aligned echo traces observed by RPI on this day, indicates that this polar cap enhancement was not limited to the vicinity of the IMAGE apogee. In the next section we

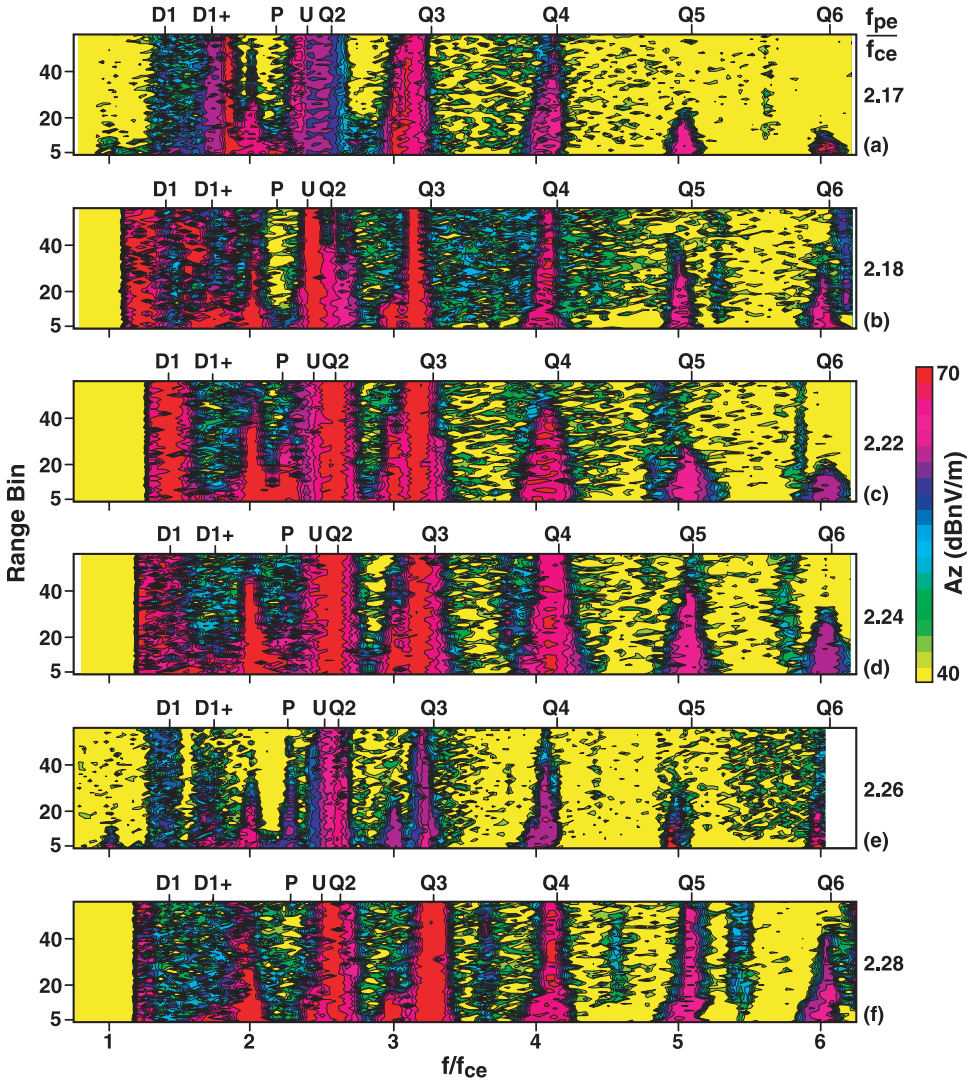

Figure 5. RPI plasmagrams normalized by f_{ce} (as determined from the RPI nfce resonances) and arranged in order (from top to bottom) of increasing f_{pe}/f_{ce} (displayed to the right of each figure) for 31 March 2001. The bottom scale indicates the normalized nf_{ce} values. (a–f) The scaled fce values used to perform this normalization were 6.90, 5.69, 5.17, 5.22, 7.96, and 5.52 kHz, respectively. The subscripts for the frequency designations of the other plasma resonances are identified at the top of each figure (where we have used P for pe and U for uh). The f_{pe}/f_{ce} values were determined from the RPI nf_{ce}, f_{pe}, and f_{uh} resonances, with guidance from the Dn and Qn resonances whose normalized calculated frequencies are indicated by tick marks at the top of each figure. The normalized plasmagrams in Figures 5a and 5e correspond to the original plasmagrams shown in Figure 4b above and Figure 5b of *Benson et al.* [2003], respectively. The UT times corresponding to the normalized plasmagrams in Figures 5a–5f are 1753:03, 2029:03, 2111:03, 2105:03, 1611:03, and 2053:03, respectively.

will compare variations in the observed solar wind parameters, as discussed in section 1.2, with variations in the observed magnetospheric parameters (shown in Figure 6) on 31 March.

3. Wind-IMAGE/RPI Comparisons

[20] The solar wind quasi-invariant QI introduced in section 1.2 and illustrated in Figures 1 and 2 is a dimensionless index based on physical parameters; namely, it represents an energy density ratio (magnetic energy density/kinetic energy density). Similarly, the magnetospheric plasma parameter f_{pe}/f_{ce} is a dimensionless parameter that represents the ratio of two fundamental frequencies characterizing the magnetospheric plasma (and is also proportional to the ratio of the electron gyroradius to the Debye radius). In section 1.2 we illustrated the value of QI as a sensitive indicator of geoeffective magnetic structures. The importance of f_{pe}/f_{ce} in characterizing sounder-stimulated plasma resonances has been known for some time; e.g., see the discussion in *Benson et al.* [2001] and references therein, but the physical implications of this dependence have not been studied adequately. In Figure 8 we compare Wind-derived QI values with time-shifted RPI-derived f_{pe}/f_{ce}

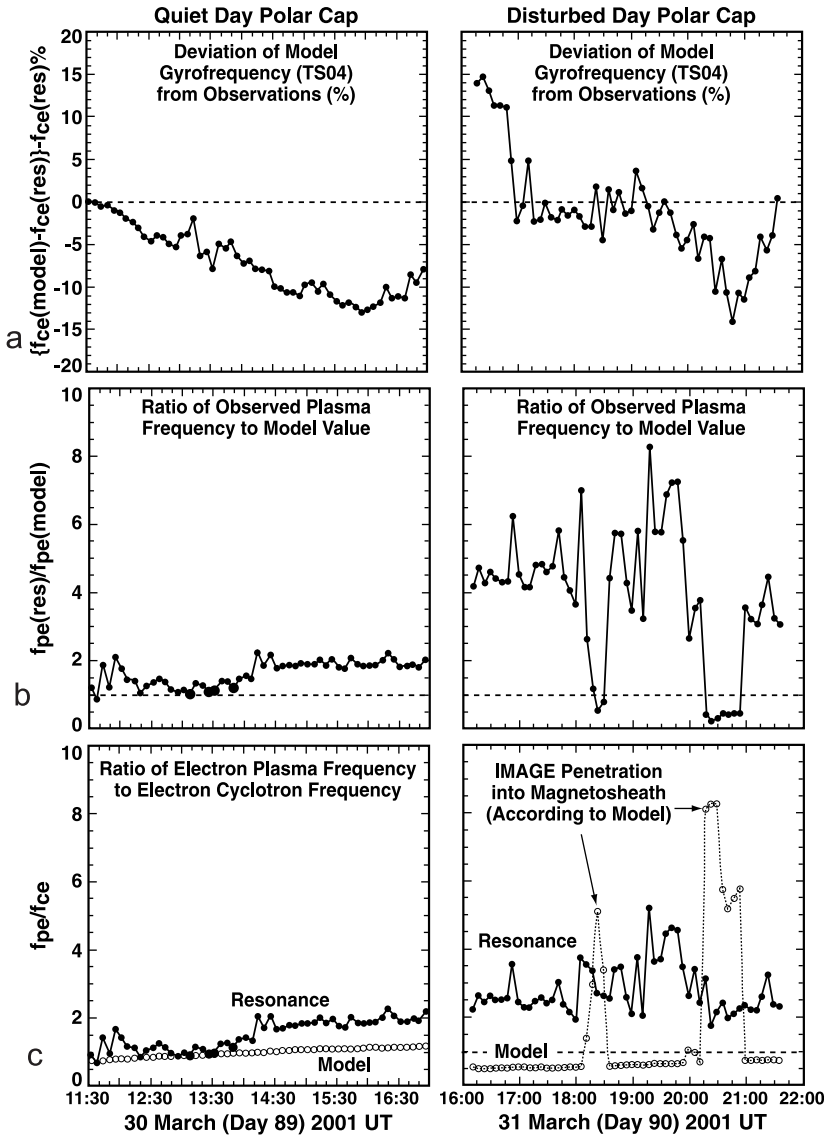

Figure 6. Comparisons between RPI/IMAGE-determined f_{pe} and f_{ce} values and model values (see text) for quiet (left) and disturbed (right) conditions. (b,c) The four larger solid dots between 1300 and 1400 UT correspond to upper limits for f_{pe}. They correspond to cases when the frequency of the f_{uh} resonance was less than the useful lower limit of 6 kHz for resonance sounding [*Benson et al.*, 2003]. (Conditions during the recording of the plasmagram in Figure 4a were approaching this limit.) Under these conditions the upper limit for f_{pe} was determined by setting f_{uh} = 6 kHz.

values for the large storm of 31 March 2001. The f_{pe}/f_{ce} values are from Figure 6c (right). They correspond to data with a resolution of 6 min, i.e., there was a 6-min interval between the high-frequency resolution RPI plasmagrams used to obtain these values. The QI values correspond to an expansion of a portion of the day 90 values in Figure 2b. They represent data with a resolution of about 2 min. A 3-hour time shift of the RPI/IMAGE data provided the good fit to the variations in QI shown in Figure 8. This delay was obtained by performing a correlation between 20-min averages of each data set as illustrated in Figure 9. With this time shift, the major variations in f_{pe}/f_{ce} as determined from plasma resonance soundings by RPI on IMAGE in the outer magnetosphere above the polar cap are seen to closely track the variations in QI as determined from Wind measurements of $|\mathbf{B}|$, ρ, and v in the solar wind. Such a time shift is comparable to typical time shifts observed between extremes in $|\mathbf{B}|$, or in *Bz*, in the solar wind and *Dst* [*Burton et al.*, 1975]. The magnitudes of the time shift in our case will depend partially on the large-scale orientation of the magnetic cloud (considered to be a magnetic flux rope [*Osherovich and Burlaga*, 1997]), relative to the spacecraft and the magnetosphere, and on the propagation speed of the expanding magnetic cloud. If Wind was located on the Sun-Earth line 250 R_E upstream from the Earth, and the magnetic cloud (flux rope) was oriented perpendicular to the Sun-Earth direction and was propagating radially from the Sun, the time shift would be about 0.7 hours for the solar wind velocity of approximately 600 km/s observed in the center of the cloud. At the time of our comparison, however,

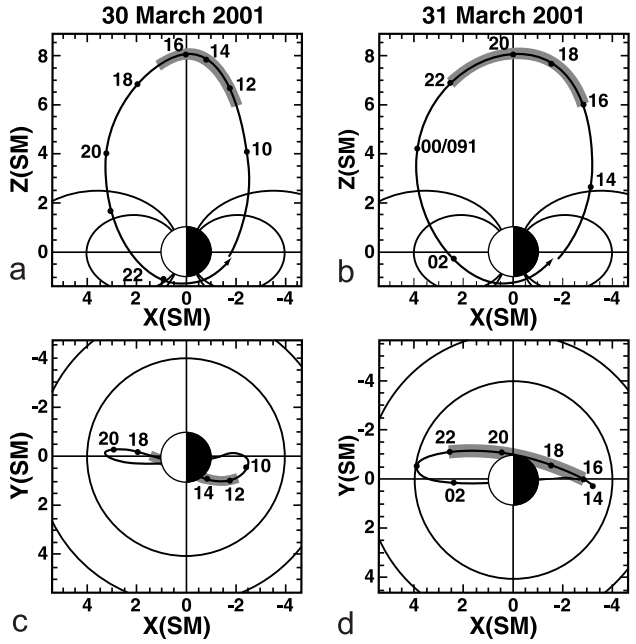

Figure 7. IMAGE locations (shaded regions) corresponding to the Figure 6 time intervals.

Wind was located off to the side of the Sun-Earth line by 250 R_E as shown in Figure 10. In this case, for a similar geometry of propagation, the time shift would be near zero. Allowing for the angle between the flux rope axis and the Sun-Earth direction to differ from 90° will result in a time shift of only a fraction of 0.7 hours. This small time delay, of much less than 1 hour, is supported by the analysis of Wind MFI magnetic field data shifted to the bow shock nose as described at omniweb.gsfc.nasa.gov/omsc_min.html. The second, and major, contribution to the time shift comes from the propagation of the disturbance inside the magnetosphere (which is of a much smaller scale than the magnetic cloud). Our present understanding of the magnetospheric plasma redistribution during a magnetic storm does not allow us to make an estimate of the time shift due to the second process. We believe that our results, however, will provide observational constraints on future models for the restructuring of the magnetosphere during major magnetic storms.

[21] The good correlation observed between the magnetospheric and solar wind measurements in spite of the large separation between the two spacecraft indicates the very large extent of the geoeffective solar wind structure in this case. Such a large size is also indicated by the typical time durations of approximately 1 day for the passage of the structures near the earth corresponding to Figure 2. Considering their 4-day travel times from the Sun, they exceed 0.2 AU (or 4500 R_E) in diameter, well beyond the scale in Figure 10.

[22] The above good correlation determination between the magnetospheric and solar wind measurements was only possible for one of the three Dst decreases identified in Figure 2a, namely, the one for 31 March 2001. During this event IMAGE was in the right place at the right time so nearly 6 hours of high-resolution RPI resonance measurements were available from the polar cap near-apogee portion of the IMAGE orbit for (time-shifted) comparison with the Wind data. Similar high-resolution RPI resonance measurements were not available during the first *Dst* decrease because high-resolution sounder-stimulated resonance measurements, of the type shown in Figures 3b and 3d based on plasmagrams like those in Figure 4, only became available after 29 March 2001 when the *Z*-channel receiver gain was significantly decreased. During the 11–12 April 2001 *Dst* decrease (centered on day 102 in Figure 2a) a time shift in the RPI data (comparable to that found for the large event of day 90 in Figure 2a) produced more than an 8-hour gap in high-resolution RPI resonance measurements (because IMAGE was far from apogee) in the center of the QI disturbance for this cloud so no comparisons were available for the central large QI peak in Figure 2b during day 102. In addition, the time-shifted RPI data for most of the interval between this QI peak and the final QI peak (near the middle of day 102) could only determine an upper limit for f_{pe}/f_{ce} because both f_{pe} and f_{uh} were below the plasmagram 6 kHz lower limit.

[23] Thus the solar wind/magnetosphere correlation determination obtained for the great magnetic storm of 31 March 2001 (see Figures 8 and 9) could be considered to represent a violation of Murphy's law in that the required receiver-gain reduction was made the day before the storm and RPI was able to collect high-frequency resolution sounder data high above the polar cap during an optimum time interval.

4. Discussion and Summary

[24] The RPI on IMAGE detected large N_e enhancements high above (8 R_E radial distance) the northern polar cap during the great magnetic storm of 31 March 2001; enhancements, though more moderate, were also observed in $|\mathbf{B}|$. The enhancements were based on measurements of the RPI sounder-stimulated plasma resonances to determine f_{pe} and f_{ce}, which are related to N_e and $|\mathbf{B}|$ by equations (1)

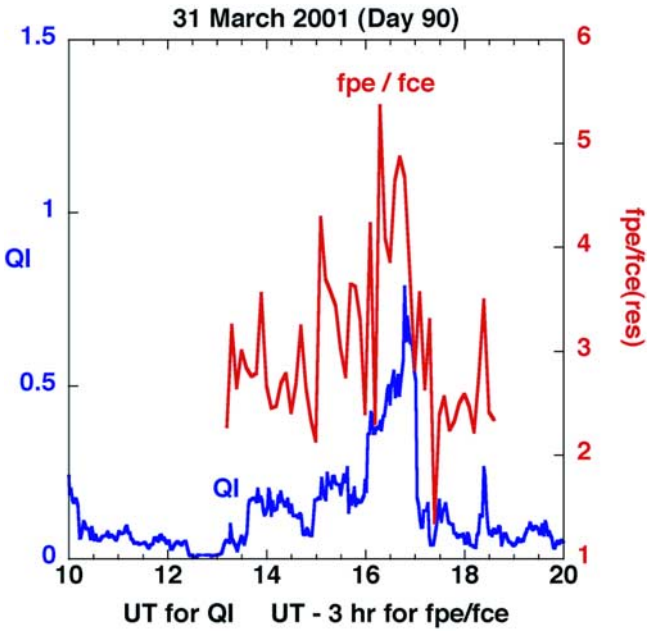

Figure 8. Comparison of solar wind QI and magnetospheric f_{pe}/f_{ce} variations (with a 3 hour time shift), as measured by RPI.

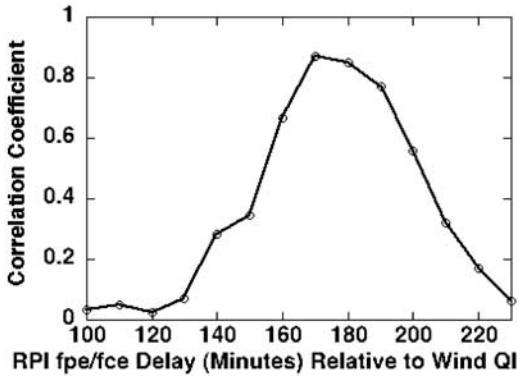

Figure 9. Correlation coefficient between the solar-wind QI and magnetospheric f_{pe}/f_{ce} variations versus time shift based on 20-min averages of each data set.

and (2), respectively, and are expressed relative to the preceding quiet day as follows: (1) f_{pe} increased by approximately a factor of 2 relative to the largest quiet day values and by approximately a factor of 4 relative to the lower background values observed on that day (corresponding to N_e enhancements by factors of ~4 and 16, respectively); (2) f_{ce} typically increases by less than a factor of 2; (3) f_{pe}/f_{ce} increased from a value comparable to the highest level from the previous day to a peak value approximately a factor of 2 higher.

[25] The f_{pe}/f_{ce} ratio varied between about one and two on the quiet day and two and five on the disturbed day; these values typically yield a rich spectrum of plasma resonances. The resulting f_{ce} and f_{pe} values were compared with the TS04 and the RPI/BinBrowser N_e models (see the first paragraph of section 2), respectively. The results indicated that: (1) f_{ce}(TS04) was within 15% of f_{ce}(res) on both quiet and disturbed days; (2) f_{pe}(res) ranged from agreement to more than a factor of two above f_{pe}(mod) on the quiet day (corresponding to N_e ranging from agreement to more than a factor of four above N_e(mod)); (3) f_{pe}(res) ranged from more than a factor of 4 to 8 f_{pe}(mod) on the disturbed day (corresponding to N_e ranging from more than a factor of 16 to 64 N_e(mod)).

[26] In addition to the solar wind index QI being highly correlated (cc = 0.98) with SSN over nearly 3 solar cycles, based on earlier work, it was shown to be well correlated with the 10.7-cm radio flux (cc = 0.85 for running 55-day averages) over a 5-year interval (see Figure 1). Also, the characteristics of solar wind QI enhancements as magnetic-cloud-induced magnetic storm indicators were reviewed and additional evidence was presented to emphasize the importance of QI in this regard (see Figure 2). Variations of the disturbed solar wind QI and the magnetspheric f_{pe}/f_{ce} values were found to be well correlated (correlation coefficient = 0.87) when a 3-hour time delay was applied to the f_{pe}/f_{ce} values. No physical explanation as to why these nondimensional parameters should track each other so well, nor why there should be a 3-hour time lag (mainly due to magnetospheric processes), was offered. It is possible that other combinations of solar wind parameters may have comparable correlation coefficients with similar time delays. In this regard, now that accurate magnetospheric f_{pe}/f_{ce} values are available, it would be interesting to use some of the functions that have been proposed to couple solar wind parameters and geomagnetic indices (like those listed in the work of *Stamper et al.* [1999]) to try to couple directly to these f_{pe}/f_{ce} values. Our focus, however, is on QI because of its unique association with SSN and its clear physical importance in the solar wind magnetohydrodynamic regime as indicated by equation (3).

[27] The above results stress the importance of accurate magnetospheric N_e measurements and suggest that, as the nondimensional parameter QI can be used as a sensitive indicator of solar wind conditions leading to magnetic storms, the nondimensional parameter f_{pe}/f_{ce} may prove to be an important indicator of the magnetospheric plasma and magnetic response to such storms.

[28] We have shown that the close tracking of the major variations in f_{pe}/f_{ce} in the outer magnetosphere above the polar cap and the variations in QI in the solar wind suggests the possibility of establishing a quantitative relation between these parameters. Such a relation between disturbed parameters in the solar wind and disturbed values of $|\mathbf{B}|$ and N_e in the magnetosphere, together with the time delay of the magnetospheric response, would provide a valuable supplement to other studies directed toward relating solar wind perturbations to variations in geomagnetic indices. More simultaneous measurements of the changes in $|\mathbf{B}|$ and N_e in the magnetosphere in response to the arrival of interplanetary disturbances are needed in order to establish such a relationship. These measurements are beyond the scope of this paper.

[29] It is important to note that the TS04 model for $\mathbf{B}$ [*Tsyganenko and Sitnov*, 2005] allows for the reconstruction of electric currents and thus the $\mathbf{J} \times \mathbf{B}$ force. It is this force that redistributes N_e (and thus the gas pressure which, in turn, is dependent on N_e) during magnetic storms. The polar cap N_e enhancement presented here, and by *Tu et al.* [2007], during the great 31 March 2001 magnetic storm taken together with the N_e decrease in the equatorial plasma-

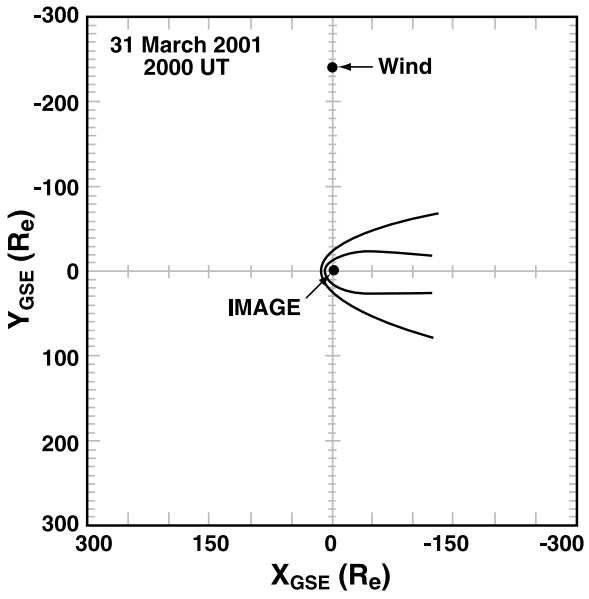

Figure 10. Relative positions of IMAGE and Wind on 31 March 2001 during the time of the comparison in Figures 8 and 9.

spheric region [*Reinisch et al.*, 2004] during the same storm are consistent with such an N_e redistribution. Thus accurate RPI f_{pe} measurements, of the type used to produce the red curve in Figure 8, can be used to provide an essential ingredient for self-consistent magnetospheric modeling, i.e., including both magnetic and plasma structures.

[30] Other solar wind parameters could be used to relate solar wind disturbances to a magnetospheric response. For example, *Moore et al.* [1999] related increases in the outflow of H^+, O^+, and He^+ ions observed by Polar to the increase in the solar wind ram pressure associated with the passage of an interplanetary shock on 24 September 1998 as observed by Wind. In our case of the 31 March 2001 storm, the increase in the observed polar cap f_{pe}/f_{ce} followed the largest increase in solar wind ram pressure related to this event by about 13 hours making an association unlikely.

[31] In space physics in general, and also in space weather forecasting, the extreme variability of measured spacecraft parameters as functions of time and position presents the problem of separating temporal and spatial effects. In the case of the solar wind the quasi-invariant combination defined by equation (3), i.e., QI, varies only slightly in space throughout the heliosphere. For example, *Fainberg and Osherovich* [2002] used Pioneer Venus Orbiter and Voyager data to demonstrate that, while the solar wind parameters B and N_p changed by several orders of magnitude between 0.7 and 28 AU, QI changed very little. Thus the close linkage found between QI and the solar cycle as measured by SSN [*Fainberg et al.*, 2001] holds throughout the heliosphere. It is this relative stability of the baseline of QI fluctuations at a given distance from the Sun that makes QI such a valuable indicator of a solar wind disturbance or anomaly such as a magnetic cloud where QI increases by a factor of 10 to 100.

[32] In the case of planetary magnetospheres the similarity of the spectrum of sounder-stimulated plasma resonances in the Earth's ionosphere and magnetosphere [*Benson et al.*, 2003] and in Jupiter's Io plasma torus [*Osherovich et al.*, 1993; *Stone et al.*, 1992], and observations indicating that this spectrum is much more sensitive to variations in f_{pe}/f_{ce} than to variations in the individual parameters f_{pe} or f_{ce}, or even T_e, [*Benson et al.*, 2001], suggests that this plasma parameter f_{pe}/f_{ce} may be considered to have a quasi-invariant nature. Even though it may vary from less than 0.2 in auroral kilometric radiation (AKR) source regions [*Benson and Calvert*, 1979] to more than 10 in the low-altitude equatorial ionosphere [*Benson*, 1972, 1974], there are extended regions in Earth's ionosphere and magnetosphere and Jupiter's Io plasma torus where this parameter is in the range from 1 to 8 in spite of much larger variations in f_{pe}, f_{ce}, and T_e between these three plasmas [*Osherovich et al.*, 2005]. Combining the present results, comparing solar wind QI and magnetospheric polar cap f_{pe}/f_{ce} variations, with these earlier findings suggests the value of creating three-dimensional f_{pe}/f_{ce} maps for magnetically quiet and disturbed times in addition to such maps for **B** and N_e.

[33] **Acknowledgments.** VAO was supported by NASA under a grant to the Catholic University of America and BWR was supported by NASA under Southwest Research Institute subcontract 83822. We acknowledge helpful comments from the reviewer and J. H. King.

[34] Zuyin Pu thanks H. Gordon James for the assistance in evaluating this paper.

References

Allen, C. W. (1973), *Astrophysical Quantities*, 3rd ed., Athlone, London.

Baker, D. (Ed.) (1986), *Statistical Analysis in the Study of Solar Wind-Magnetosphere Coupling*, pp.17–38, Terra Sci, Tokyo.

Benson, R. F. (1972), Ionospheric plasma resonances: Time durations vs. latitude, altitude, and fN/fH, *Planet. Space Sci.*, *20*, 683–706.

Benson, R. F. (1974), Stimulation of the Harris instability in the ionosphere, *Phys. Fluids*, *17*, 1032–1037.

Benson, R. F. (1977), Stimulated plasma waves in the ionosphere, *Radio Sci.*, *12*, 861–878.

Benson, R. F. (1982), Stimulated plasma instability and nonlinear phenomena in the ionosphere, *Radio Sci.*, *17*, 1637–1659.

Benson, R. F., and W. Calvert (1979), ISIS 1 observations at the source of auroral kilometric radiation, *Geophys. Res. Lett.*, *6*, 479–482.

Benson, R. F., V. A. Osherovich, J. Fainberg, A.-F. Vinas, and D. R. Ruppert (2001), An interpretation of banded magnetospheric radio emissions, *J. Geophys. Res.*, *106*, 13,179–13,190.

Benson, R. F., V. A. Osherovich, J. Fainberg, and B. W. Reinisch (2003), Classification of IMAGE/RPI-stimulated plasma resonances for the accurate determination of magnetospheric electron-density and magnetic field values, *J. Geophys. Res.*, *108*(A5), 1207, doi:10.1029/2002JA009589.

Burch, J. L. (2000), IMAGE mission overview, *Space Sci. Rev.*, *91*, 1–14.

Burton, R. K., R. L. McPherron, and C. T. Russell (1975), An empirical relationship between interplanetary conditions and Dst, *J. Geophys. Res.*, *80*, 4204–4214.

Cliver, E. W., A. G. Ling, J. E. Wise, and L. J. Lanzerotti (1999), A prediction of geomagnetic activity for solar cycle 23, *J. Geophys. Res.*, *104*, 6871–6876.

Donley, J. L., L. H. Brace, J. A. Findlay, J. H. Hoffman, and G. L. Wrenn (1969), Comparison of results of Explorer XXXI direct measurement probes, *Proc. IEEE*, *57*, 1078–1084.

Fainberg, J., and V. A. Osherovich (2002), Solar wind quasi-invariant as a heliospheric index of solar activity, in *Proceedings of 10th European Solar Phys. Meeting "Solar Variability: From Core to Outer Frontiers,"* edited by A. Wilson, *Eur. Space Agency Spec. Publ., ESA SP-506*, 43–45.

Fainberg, J., V. A. Osherovich, and R. G. Stone (2001), Pioneer-Venus observations of a solar wind quasi-invariant, *Geophys. Res. Lett.*, *28*, 1447–1449.

Feynman, J. (1983), Solar cycle and long-term changes in the solar wind, *Rev. Geophys.*, *21*, 338–348.

Galkin, I. A., G. Khmyrov, A. Kozlov, B. W. Reinisch, X. Huang, and G. Sales (2001), New tools for analysis of space-borne sounding data, paper presented at 2001 USNC/URSI National Radio Science Meeting, IEEE, Boston.

Hathaway, D. H. (1998), Synoptic datasets and solar activity predictions, in *Synoptic Solar Physics*, *Conf. Ser.*, vol. 140, edited by K. S. Basubramaniam, J. W. Harvey, and D. M. Rabin, pp. 47–55, Am. Soc. of Phys., San Francisco, Calif.

Horne, R. B., R. M. Thorne, N. P. Meredith, and R. R. Anderson (2003), Diffuse auroral electron scattering by electron cyclotron harmonic and whistler mode waves during an isolated substorm, *J. Geophys. Res.*, *108*(A7), 1290, doi:10.1029/2002JA009736.

King, J. H. (1979), Solar cycle variations in IMF intensity, *J. Geophys. Res.*, *84*, 5938–5940.

Moore, T. E., W. K. Peterson, C. T. Russell, M. O. Chandler, M. R. Collier, H. L. Collin, P. D. Craven, R. Fitzenreiter, B. L. Jiles, and C. J. Pollock (1999), Ionospheric mass ejection in response to a CME, *Geophys. Res. Lett.*, *26*, 2339–2342.

Osherovich, V. A., and L. F. Burlaga (1997), Magnetic Clouds, in *Coronal Mass Ejections*, *Geophys. Monogr. Ser.*, vol. 99, edited by N. Crooker, J. A. Joselyn, and J. Feynman, pp. 157–168, AGU, Washington, D. C.

Osherovich, V. A., R. F. Benson, J. Fainberg, R. G. Stone, and R. J. MacDowall (1993), Sounder stimulated Dn Resonances in Jupiter's Io plasma torus, *J. Geophys. Res.*, *98*, 18,751–18,756.

Osherovich, V. A., J. Fainberg, R. G. Stone, and D. B. R. J. MacDowall (1997), Self-similar evolution of interplanetary magnetic clouds and Ulysses measurements of the polytropic index inside the cloud, paper presented at Correlated Phenomena at the Sun in the Heliosphere and in Geospace, Eur. Space Agency, Noordwijk, Netherlands.

Osherovich, V. A., J. Fainberg, and R. G. Stone (1999a), Multi-tube model for interplanetary magnetic clouds, *Geophys. Res. Lett.*, *26*, 401–404.

Osherovich, V. A., J. Fainberg, and R. G. Stone (1999b), Solar wind quasi-invariant as a new index of solar activity, *Geophys. Res. Lett.*, *26*, 2597–2600.

Osherovich, V. A., R. F. Benson, and J. Fainberg (2005), Electromagnetic bounded states and challenges of plasma spectroscopy, *IEEE Trans. Plasma Sci.*, *33*, 599–608.

Pap, J., L. Floyd, R. B. Lee, D. Parker, L. Puga, R. Ulrich, F. Varadi, and R. Viereck (1997), Long term variations in total solar and uv irradiance, in *The 31st ESLAB Symposium on Correlated Phenomena at the Sun, in the Heliosphere and in Geospace*, edited by A. Wilson, *Eur. Space Agency Spec. Publ., ESA SP-415*, 251–257.

Persoon, A. M., D. A. Gurnett, and S. D. Shawhan (1983), Polar cap electron densities from DE 1 plasma wave observations, *J. Geophys. Res.*, *88*, 10,123–10,136.

Reinisch, B. W., et al. (2000), The radio plasma imager investigation on the IMAGE spacecraft, *Space Sci. Rev.*, *91*, 319–359.

Reinisch, B. W., et al. (2001), First results from the radio plasma imager on IMAGE, *Geophys. Res. Lett.*, *28*, 1167–1170.

Reinisch, B. W., X. Huang, P. Song, J. L. Green, S. F. Fung, V. M. Vasyliunas, D. L. Gallagher, and B. R. Sandel (2004), Plasmaspheric mass loss and refilling as a result of a magnetic storm, *J. Geophys. Res.*, *109*, A01202, doi:10.1029/2003JA009948.

Roelof, E. C., and D. G. Sibeck (1993), Magnetopause shape as a bivariate function of interplanetary magnetic field Bz and solar wind dynamic pressure, *J. Geophys. Res.*, *98*, 21,421–21,450. (Correction, *J. Geophys. Res.*, *98*, 21,499.)

Seki, K., M. Hirahara, M. Hoshino, T. Terasawa, R. C. Elphic, Y. Saito, T. Mukai, H. Hayakawa, H. Kojima, and H. Matsumoto (2003), Cold ions in the hot plasma sheet of Earth's magnetotail, *Nature*, *422*, 589–592.

Slavin, J. A., G. Jungman, and E. J. Smith (1986), The interplanetary magnetic field during solar cycle 21: ISEE-3/ICE observations, *Geophys. Res. Lett.*, *13*, 513–516.

Stamper, R., M. Lockwood, M. N. Wild, and T. D. G. Clark (1999), Solar causes of the long-term increase in geomagnetic activity, *J. Geophys. Res.*, *104*, 28,325–28,342.

Stone, R. G., et al. (1992), Ulysses radio and plasma wave observations in the Jupiter environment, *Science*, *257*, 1524–1531.

Tsyganenko, N. A. (1995), Modeling the Earth's magnetospheric magnetic field confined within a realistic magnetopause, *J. Geophys. Res.*, *100*, 5599–5612.

Tsyganenko, N. A. (1996), Effects of the solar wind conditions on the global magnetospheric configuration as deduced from data-based field models, in *Third International Conference on Substorms (ICS-3)*, edited by E. Rolfe and B. Kaldeich, *Eur. Space Agency Spec. Publ., ESA SP-389*, 181.

Tsyganenko, N. A., and M. I. Sitnov (2005), Modeling the dynamics of the inner magnetosphere during strong geomagnetic storms, *J. Geophys. Res.*, *110*, A03208, doi:10.1029/2004JA010798.

Tsyganenko, N. A., and D. P. Stern (1996), Modeling the global magnetic field of the large-scale Birkeland current systems, *J. Geophys. Res.*, *101*, 27,187–127,198.

Tu, J.-N., M. Dhar, P. Song, B. W. Reinisch, J. L. Green, R. F. Benson, and A. J. Coster (2007), Extreme polar cap density enhancements along magnetic field lines in the polar cap during an intense geomagnetic storm, *J. Geophys. Res.*, *112*, A05201, doi:10.1029/2006JA012034.

Viñas, A. F., R. L. Mace, and R. F. Benson (2005), Dispersion characteristics for plasma resonances of Maxwellian and Kappa distribution plasmas and their comparisons to the IMAGE/RPI observations, *J. Geophys. Res.*, *110*, A06202, doi:10.1029/2004JA010967.

R. F. Benson and J. Fainberg, NASA Goddard Space Flight Center, Mail Code 673 Greenbelt, MD 20771, USA. (robert.f.benson@nasa.gov; joseph.fainberg@nasa.gov)

S. Boardsen and N. Tsyganenko, NASA Goddard Space Flight Center, Mail Code 674, Greenbelt, MD 20771, USA. (scott.a.boardsen.1@gsfc.nasa.gov; nikolai.tsyganenko@gsfc.nasa.gov)

L. Garcia, NASA Goddard Space Flight Center, Mail Code 672, Greenbelt, MD 20771, USA. (leonard.n.garcia.1@gsfc.nasa.gov)

J. G. Green, NASA Headquarters, Mail Suite 3Z74, 300 E Street NW, Washington, DC 20546-0001, USA. (james.green@nasa.gov)

V. A. Osherovich, NASA Goddard Space Flight Center, Mail Code 695 Greenbelt, MD 20771, USA. (vladimir.a.osherovich.1@gsfc.nasa.gov)

B. W. Reinisch, Environmental, Earth and Atmospheric Sciences Department, Center for Atmospheric Research, University of Massachusetts Lowell, Lowell, MA 01854, USA. (bodo_reinisch@uml.edu)